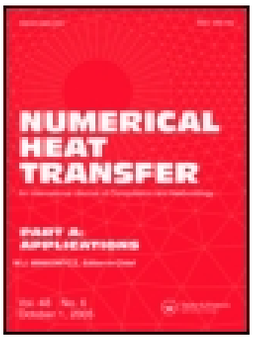

Numerical Heat Transfer, Part A: Applications

ISSN: 1040-7782 (Print) 1521-0634 (Online) Journal homepage: www.tandfonline.com/journals/unht20

BUOYANCY-AIDED MIXED CONVECTION WITH CONDUCTION AND SURFACE RADIATION FROM A VERTICAL ELECTRONIC BOARD WITH A TRAVERSABLE DISCRETE HEAT SOURCE

C. Gururaja Rao

To cite this article: C. Gururaja Rao (2004) BUOYANCY-AIDED MIXED CONVECTION WITH CONDUCTION AND SURFACE RADIATION FROM A VERTICAL ELECTRONIC BOARD WITH A TRAVERSABLE DISCRETE HEAT SOURCE, Numerical Heat Transfer, Part A: Applications, 45:9, 935-956, DOI: 10.1080/10407780490439202

To link to this article: https://doi.org/10.1080/10407780490439202

Published online: 17 Aug 2010.

Numerical Heat Transfer, Part A, 45: 935–956, 2004

ISSN: 1040-7782 print/1521-0634 online
DOI: 10.1080/10407780490439202

Taylor & Francis
Taylor & Francis Group

BUOYANCY-AIDED MIXED CONVECTION WITH CONDUCTION AND SURFACE RADIATION FROM A VERTICAL ELECTRONIC BOARD WITH A TRAVERSABLE DISCRETE HEAT SOURCE

C. Gururaja Rao
Department of Mechanical Engineering, National Institute of Technology, [Formerly, Regional Engineering College Warangal], Warangal, India

This article presents the results of a comprehensive fundamental numerical study of the problem of buoyancy-aided mixed convection with conduction and surface radiation from a vertical electronic board provided with a traversable, flush-mounted, discrete heat source. Air, a radiatively transparent medium, is considered to be the cooling agent. The governing equations in primitive variables for fluid flow and heat transfer are first converted into stream function–vorticity form, and are later converted into algebraic form using the finite-volume method. The resulting finite-difference equations are solved by Gauss-Seidel iterative technique. The governing equation for temperature distribution along the electronic board is obtained by appropriate energy balance. The effects of pertinent parameters, viz., location of the discrete heat source, surface emissivity of the board, and modified Richardson number, on various results, including local temperature distribution along the board, maximum board temperature, and contributions of convection and surface radiation to heat dissipation from the board, are studied in great detail. The fact that any design calculation that ignores surface radiation in problems of this kind would be error-prone is clearly highlighted.

INTRODUCTION

Multimode heat transfer continues to be a fertile area of research because of its role in several fields, including the cooling of electronic equipment and the design of solar collectors. With regard to electronic equipment cooling, vertical board-mounted electronic components are typically cooled by the removal of the heat generated in the components using air as one of the most promising cooling agents. In most of these applications, there will invariably be an interaction of buoyancy-aided mixed (combined free and forced) convection with conduction and surface radiation.

Studies on mixed convection that involve conduction and (or) surface radiation seem to be relatively few. Among the earliest works reported on multimode heat transfer for the vertical plate geometry is the one of Zinnes [1]. He investigated

Received 13 June 2003; accepted 1 December 2003.
Address correspondence to C. Gururaja Rao, Department of Mechanical Engineering, National Institute of Technology, Warangal 506 004, India. E-mail: cgrr@nitw.ernet.in

NOMENCLATURE

A_1	nondimensional heat source position in the electronic board ($=L_1/L$)	t	thickness of the electronic board as well as the discrete heat source, m
A_{r_1}, A_{r_2}	geometric ratios, defined as (L/t), (L/L_h), respectively	T	temperature at any location in the computational domain, K
$\overline{C}_f$	mean friction coefficient $[=(2/\mathrm{Re}_L)\int_0^1(\partial U/\partial Y)_{Y=0}\,dX]$	T_w	uniform surface temperature of the vertical board in the asymptotic limit, K
g	acceleration due to gravity ($=9.81$ m/s^2)	T_∞	free-stream temperature of the fluid, K
Gr_L	Grashof number based on L $[=g\beta(T_w-T_\infty)L^3/\nu^2]$	u	vertical velocity, m/s
Gr_L^*	modified Grashof number based on L ($=g\beta\Delta T_{\mathrm{ref}}L^3/\nu^2$)	u_∞	free-stream velocity of the fluid, m/s
h_x	local convection heat transfer coefficient defined for asymptotic case, W/m^2 K	U	nondimensional vertical velocity ($=u/u_\infty$ or $\partial\psi/\partial Y$)
		v	horizontal or cross velocity, m/s
H, W	height and width of the computational domain, respectively, m	V	nondimensional horizontal or cross velocity ($=v/u_\infty$ or $-\partial\psi/\partial X$)
k	thermal conductivity, W/m K	x, y	vertical and horizontal distances, respectively, m
L	height of the electronic board, m		
L_h	height of the discrete heat source, m	X, Y	nondimensional vertical and nondimensional horizontal distances (x/L, y/L, respectively)
L_1	heat source position in the board, m	α	thermal diffusivity of the fluid, m^2/s
M, N	number of grid points in horizontal and vertical directions, respectively	β	isobaric cubic expansivity of the fluid $\left[=-(1/\rho)(\partial\rho/\partial T)_P\right]$, 1/K
N_1	number of grid points along the electronic board	γ	thermal conductance parameter $\left(=k_fL/k_st\right)$
N_{RF}	radiation-flow interaction parameter $\left\{=\sigma T_\infty^4\Big/[(\mathrm{k_f/L})\,\Delta T_{\mathrm{ref}}]\right\}$	δ_c	convergence criterion, in fractional form $[=\lvert(\zeta_{\mathrm{new}}-\zeta_{\mathrm{old}})/\zeta_{new}\rvert]$
		ΔT_{ref}	modified reference temperature difference $[=q_vL_ht/k_s]$, K
Nu_x	local Nusselt number along the board defined for the asymptotic case ($=h_xx/k_f$)	Δx	height of the board element chosen for energy balance, m
P	pressure at any location in the computational domain, Pa	ΔX	nondimensional height of the board element ($=\Delta x/L$)
Pe_L	Peclet number based on L $[(\mathrm{Re}_L\,\mathrm{Pr})$ or $(u_\infty L/\alpha)]$	Δy	horizontal distance measured between any grid point along the board and its adjacent grid point, m
Pr	Prandtl number ($=\nu/\alpha$)		
q_V	volumetric heat generation in the discrete heat source, W/m^3	ΔY	nondimensional horizontal distance between any grid point along the board and its adjacent grid point ($=\Delta y/L$)
Q	rate of heat transfer, W		
Re_L	Reynolds number based on L ($=u_\infty L/\nu$)		
Ri_L	Richardson number based on L $\{=\left(\mathrm{Gr}_L/\mathrm{Re}_L^2\right)$ or $\left[g\beta(T_w-T_\infty)L/u_\infty^2\right]\}$	ε	surface emissivity of the electronic board
		θ	nondimensional temperature at any location in the computational domain $\{=(T-T_\infty)/\Delta T_{\mathrm{ref}}$ [or $(T-T_\infty)/(T_w-T_\infty)$ in the asymptotic limiting case]$\}$
Ri_L^*	modified Richardson number based on L $\left[=\left(\mathrm{Gr}_L^*/\mathrm{Re}_L^2\right)\right.$ or $\left.(g\beta\,\Delta T_{\mathrm{ref}}\,L/u_\infty^2)\right]$		

ζ	any variable (ψ, ω, or θ), over which convergence is being tested for	**Subscripts**	
		av, max	average and maximum temperatures of the electronic board, respectively
ν	kinematic viscosity of the fluid, m^2/s		
ρ	density of the fluid, kg/m^3		
ρ_c	characteristic density of the fluid, kg/m^3	cond, conv	conduction and convection, respectively
σ	Stefan-Boltzmann constant ($=5.6697\times10^{-8}$ W/m^2 K^4)	*f*, *s*	fluid and solid (board material), respectively
ω'	vorticity, 1/s	new, old	values of the dependent variable (ψ, ω, or θ) obtained from the present and previous iterations, respectively
ω	nondimensional vorticity [$=(\omega' L/u_\infty)$ or $(\omega' S/u_\infty)$]		
ψ'	stream function, m^2/s		
ψ	nondimensional stream function [$=(\psi'/u_\infty L)$ or $(\psi'/u_\infty S)$, problem − specific]	*P*	local temperature along the board
		rad	radiation

steady, constant-property, two-dimensional, laminar natural convection from a vertical, heat-conducting, flat plate of finite thickness with an arbitrary heating distribution on its surface. Tewari and Jaluria [2] conducted an experimental study on the fundamental aspects of conjugate mixed convection from two heat sources of finite width and negligible thickness and having a uniform heat flux input at the surface. Gorski and Plumb [3] investigated, numerically, the problem of conjugate laminar forced convection from a single discrete heat source, flush-mounted on a flat plate. Kishinami et al. [4, 5] made a numerical and experimental study of laminar mixed convection from a vertical composite plate, provided with isolated, discontinuous, surface heating elements. They simplified the problem by neglecting heat conduction in the unheated portion of the plate.

Hossain and Takhar [6] did a numerical study of the effect of surface radiation on combined forced and free convection from a heated vertical flat plate for the case of uniform free-stream and uniform surface temperatures. Here, the governing boundary-layer equations were first reduced to local nonsimilarity equations, which were later solved through an implicit finite-difference method. Vynnycky and Kimura [7] investigated, both analytically and numerically, two-dimensional conjugate free convection from a vertical plate in communication with a semi-infinite fluid region. Merkin and Pop [8] numerically solved conjugate free convection from a vertical surface, in which the governing boundary-layer equations for fluid flow were made dimensionless, involving only the Prandtl number. Cole [9] numerically solved the problem of electronic cooling during the steady flow of a viscous fluid over a heated strip on a flat plate using the principles of scaling. Wang et al. [10] investigated, numerically, using a multigrid technique, the two-dimensional, conjugate, laminar natural-convection air cooling of a vertical plate, provided with five wall-attached, protruding, discretely heated integrated circuit (IC) packages. Kimura et al. [11] probed, analytically and experimentally, into the problem of conjugate laminar as well as turbulent natural convection from a vertical plate. Mendez and Trevino [12] did a numerical study of conjugate natural convection from a thin vertical strip with nonuniform internal heat generation.

The foregoing survey of literature on multimode heat transfer based on the vertical plate geometry reveals the following points. No available study seems to address, in sufficient detail, the effect of surface radiation on conjugate buoyancy-aided mixed convection from a vertical electronic board provided with a traversable flush-mounted discrete heat source. Keeping the above in mind, the present article aims at probing into multimode heat dissipation from a vertical, heat-conducting, electronic board, equipped with a flush-mounted discrete heat source that could take up any position (starting from the leading edge to the trailing edge) along the board.

MATHEMATICAL FORMULATION

The schematic of the problem geometry, which consists of a vertical electronic board with a flush-mounted discrete heat source, along with the system of coordinates, is shown in Figure 1*a*. The electronic board is of height L and thickness t. The board has a thermal conductivity k_s and surface emissivity ε. The discrete heat source is of height L_h and thickness t, which is the same as that of the board itself. The heat source is located at a distance L_1 from the leading edge of the board. The heat source here is traversable, i.e., it may take up any position along the board, starting from its leading edge [i.e., $L_1 = 0$] to the trailing edge [i.e., $L_1 = (L - L_h)$]. Heat is generated in the discrete heat source at a uniform rate of q_V W/m^3, which may be varied. The heat generated in the heat source is lost to the flowing fluid (air) directly by buoyancy-aided mixed convection and surface radiation, as well as indirectly by conduction into the board and by mixed convection and surface radiation thereafter from the board surface. Air is considered to possess constant thermophysical properties, with the Boussinesq approximation assumed valid. The basic equations governing the fluid flow and heat transfer are the equation of continuity, the two momentum equations, and the equation of energy. These equations, in terms of primitive variables, are

$$\frac{\partial u}{\partial x} + \frac{\partial v}{\partial y} = 0 \tag{1}$$

$$u\frac{\partial u}{\partial x} + v\frac{\partial u}{\partial y} = -\frac{1}{\rho}\frac{\partial P}{\partial x} + g\frac{\rho_c}{\rho} + \nu\left(\frac{\partial^2 u}{\partial x^2} + \frac{\partial^2 u}{\partial y^2}\right) - g \tag{2}$$

$$u\frac{\partial v}{\partial x} + v\frac{\partial v}{\partial y} = -\frac{1}{\rho}\frac{\partial P}{\partial y} + \nu\left(\frac{\partial^2 v}{\partial x^2} + \frac{\partial^2 v}{\partial y^2}\right) \tag{3}$$

$$u\frac{\partial T}{\partial x} + v\frac{\partial T}{\partial y} = \alpha\left(\frac{\partial^2 T}{\partial x^2} + \frac{\partial^2 T}{\partial y^2}\right) \tag{4}$$

The Navier-Stokes equations, viz., Eqs. (2) and (3), are converted into stream function–vorticity form, and this results in

$$u\frac{\partial \omega'}{\partial x} + v\frac{\partial \omega'}{\partial y} = -g\beta\frac{\partial T}{\partial y} + \nu\left(\frac{\partial^2 \omega'}{\partial x^2} + \frac{\partial^2 \omega'}{\partial y^2}\right) \tag{5}$$

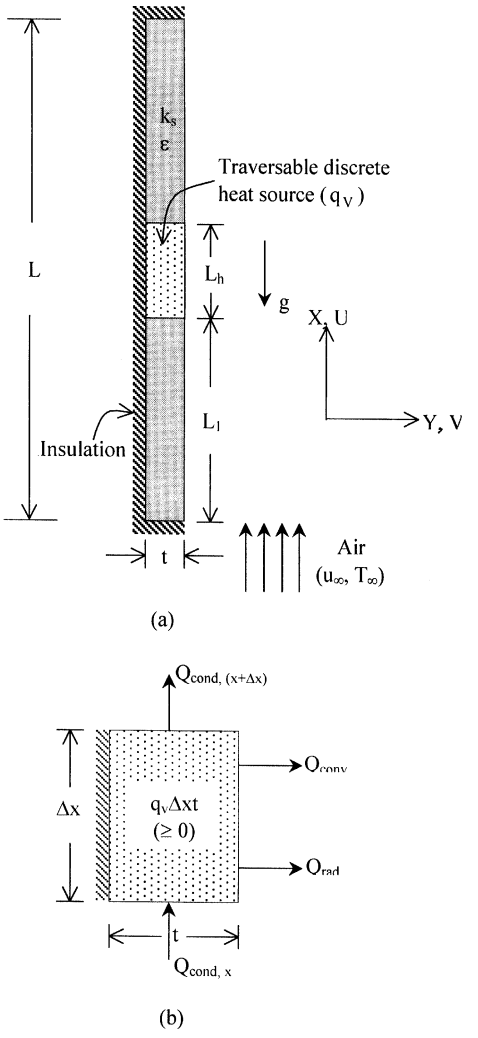

Figure 1. (*a*) Schematic of the problem geometry considered in the present study and (*b*) typical element chosen for demonstrating energy balance.

Substitution of the definitions for u and v (in terms of ψ') into the definition for ω' gives

$$\frac{\partial^2 \psi'}{\partial x^2} + \frac{\partial^2 \psi'}{\partial y^2} = -\omega' \tag{6}$$

Thus, the final set of governing equations for the present problem comprises the vorticity–transport equation [Eq. (5)], the stream-function equation [Eq. (6)], and the undisturbed energy equation [Eq. (4)]. The above governing equations are later normalized, and during this normalization, since no obvious reference temperature difference exists here, a modified reference temperature difference is introduced as

$\Delta T_{ref} = q_v L_h t/k_s$. This helps in defining a nondimensional temperature as $\theta = (T - T_\infty)/\Delta T_{\text{ref}}$. The normalized governing equations turn out to be

$$U\frac{\partial \omega}{\partial X} + V\frac{\partial \omega}{\partial Y} = -\text{R}i_L^*\frac{\partial \theta}{\partial Y} + \frac{1}{\text{Re}_L}\left(\frac{\partial^2 \omega}{\partial X^2} + \frac{\partial^2 \omega}{\partial Y^2}\right) \tag{7}$$

$$\frac{\partial^2 \psi}{\partial X^2} + \frac{\partial^2 \psi}{\partial Y^2} = -\omega \tag{8}$$

$$U\frac{\partial \theta}{\partial X} + V\frac{\partial \theta}{\partial Y} = \frac{1}{\text{Pe}_L}\left(\frac{\partial^2 \theta}{\partial X^2} + \frac{\partial^2 \theta}{\partial Y^2}\right) \tag{9}$$

It is pertinent to note that the modified Richardson number (Ri_L^*) in Eq. (7) is based on the modified reference temperature difference introduced above. Ri_L^* assumes the role of the parameter governing mixed convection, with larger values of it signifying free-convection dominance and smaller values of it implying the dominance of forced convection. A value of $\text{Ri}_L^* \approx 1$ means the mixed-convection regime with buoyancy and inertial forces becoming comparable.

COMPUTATIONAL DOMAIN AND BOUNDARY CONDITIONS

The computational domain is extended beyond the trailing edge of the board by a height equal to that of the board (L). The width (W) of the computational domain is taken equal to the board height (L) itself. The above dimensions for the computational domain have been decided based on some initial studies, the results of which will be summarized at a later stage. The computational domain, along with all the boundary conditions therein, is as shown in Figure 2.

Since the fluid enters from the bottom with a uniform velocity u_∞, it follows that $(\partial\psi/\partial Y) = 1$ or $\psi = Y$. The vorticity (ω) is taken equal to zero along the bottom boundary, which means the flow is irrotational there. With regard to temperature at the bottom, since the fluid enters at uniform temperature T_∞, the nondimensional temperature $\theta = 0$. The left boundary comprises two sections, the bottom half is the vertical board itself (solid boundary), while the top half is the extended length (free or open boundary). With regard to boundary conditions along the board, the stream function (ψ) is taken equal to zero. For vorticity (ω), the same condition as used by Gururaja Rao et al. [13] is used, i.e., $\omega = -\partial^2\psi/\partial Y^2$. The temperature boundary condition along the electronic board is derived using a simple energy balance. For example, consider a typical element, pertaining to the region along the board (excluding the bottom and top insulated ends), which possesses the discrete heat source, is as shown in Figure 1*b*, along with various energy interactions it is involved in. The energy balance on this element leads to

$$Q_{\text{cond},x} + q_v\,\Delta x\,t = Q_{\text{cond},(x+\Delta x)} + Q_{\text{conv}} + Q_{\text{rad}} \tag{10}$$

Using Taylor's series expansion for the first term on the right side of Eq. (10) and substituting relevant expressions for the other terms, one gets

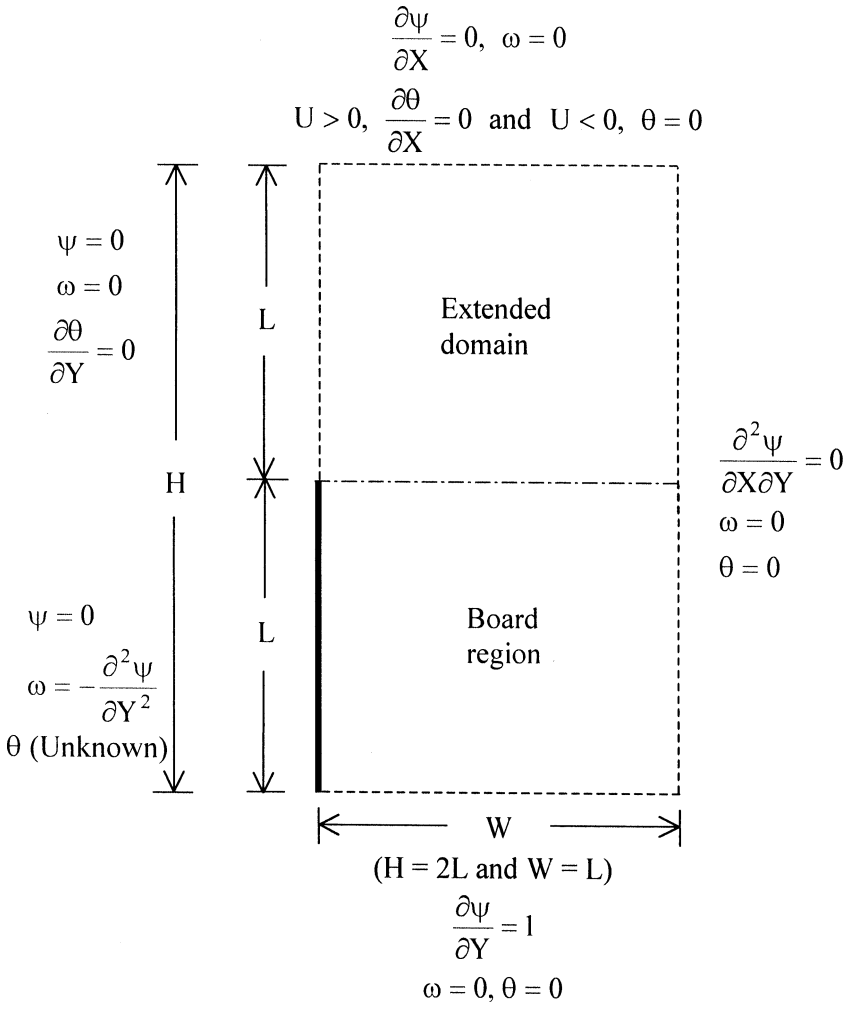

Figure 2. Computational domain used in the present study, along with boundary conditions.

$$Q_{\text{cond},x} + q_v\,\Delta x\,t = \left(Q_{\text{cond},x} + \frac{\partial Q_{\text{cond},x}}{\partial x}\,\Delta x\right) + \left[-k_f\left(\frac{\partial T}{\partial y}\right)_{y=0}\Delta x\right] + \left[\sigma\varepsilon\left(T^4 - T_\infty^4\right)\Delta x\right] \tag{11}$$

Simplification and appropriate nondimensionalization leads Eq. (11) to the governing equation for temperature distribution for the region along the board, without the bottom and top insulated ends and possessing the discrete heat source, as

$$\frac{\partial^2\theta}{\partial X^2} + \gamma\left(\frac{\partial\theta}{\partial Y}\right)_{Y=0} + A_{r_1}A_{r_2} - \varepsilon\gamma N_{\text{RF}}\left[\left(\frac{T}{T_\infty}\right)^4 - 1\right] = 0 \tag{12}$$

For the remainder of the board (other than the top and bottom ends), the energy balance gives

$$\frac{\partial^2\theta}{\partial X^2}+\gamma\left(\frac{\partial\theta}{\partial Y}\right)_{Y=0}-\varepsilon\gamma N_{\mathrm{RF}}\left[\left(\frac{T}{T_\infty}\right)^4-1\right]=0 \tag{13}$$

The governing equations for the temperatures of the bottom and top insulated ends of the board, respectively, are obtained by making energy balance on the semi-elements pertaining to these ends, and these turn out to be

$$\left(\frac{\partial\theta}{\partial X}\right)_{X=0}+\frac{(\Delta X)_{X=0}}{2}\gamma\left(\frac{\partial\theta}{\partial Y}\right)_{Y=0}+A_{r_1}A_{r_2}\frac{\Delta X}{2}-\varepsilon\gamma N_{\mathrm{RF}}\frac{\Delta X}{2}\left[\left(\frac{T}{T_\infty}\right)^4-1\right]=0 \tag{14}$$

$$\left(\frac{\partial\theta}{\partial X}\right)_{X=1}-\frac{(\Delta X)_{X=1}}{2}\gamma\left(\frac{\partial\theta}{\partial Y}\right)_{Y=0}-A_{r_1}A_{r_2}\frac{\Delta X}{2}+\varepsilon\gamma N_{\mathrm{RF}}\frac{\Delta X}{2}\left[\left(\frac{T}{T_\infty}\right)^4-1\right]=0 \tag{15}$$

The third term in Eqs. (14) and (15), which corresponds to heat generation, would be absent in all those cases, where the bottom and top ends do not form part of the discrete heat source. It is to be remembered that the heat source in the present problem is traversable and thus may or may not be at the ends of the board. With regard to extended length, because of symmetry, the cross or horizontal velocity $(V)=0$. This means that $(\partial\psi/\partial X)=0$, and this, in turn, implies that ψ is a constant along the extended left boundary. Since $\psi=0$ along the board, the same condition is also used for the extended length of the left boundary. Based on the definition of ω, it follows that $\omega=0$ on the extended left boundary, implying irrotationality condition. With regard to temperature, $(\partial\theta/\partial Y)=0$ satisfies the symmetry condition. At the top boundary, it is assumed that the stream function satisfies the fully developed condition, viz., $(\partial\psi/\partial X)=0$. For vorticity, since the computational domain is extended well beyond the trailing edge of the board (by a height equal to the board height) along the flow direction, irrotationality is satisfied along the top, which implies $\omega=0$. With regard to temperature (θ), when the vertical velocity (U) is positive, the fully developed condition, viz., $(\partial\theta/\partial X)=0$, is appropriate. Conversely, when U is negative, indicating an incoming flow, the temperature is taken equal to that of the free stream, implying $\theta=0$. As far as the right free (open) boundary is concerned, three different options are possible for specifying the stream function, and all of them have been tried in the present study, to converge on the option that best suites the entire mixed-convection regime. The first option is to assume the cross velocity $(V)=0$, implying $(\partial\psi/\partial X)=0$. The second possibility is to consider the vertical velocity $(U)=0$, which means $(\partial\psi/\partial Y)=0$. Both of the above appear justifiable from a physical standpoint—the former in the asymptotic forced-convection

limit and the latter in the asymptotic free-convection limit. However, since the present study encompasses the whole range of mixed convection (forced, mixed, and free), neither of the above conditions is appropriate. Instead, the best possible option is a less restrictive condition on the stream function that is given as $(\partial U/\partial X) = (\partial V/\partial Y) = \left(\partial^2\psi/\partial X\partial Y\right) = 0$. With regard to vorticity, since the right boundary is far away from the board (by a distance equal to the board height), the flow can be assumed irrotational, i.e., $\omega = 0$. Using similar arguments, the temperature on the right boundary is equal to the free-stream temperature (T_∞) (i.e., $\theta = 0$).

GRID SYSTEM

The temperature variation along the electronic board depends on the height (L_h) and also the position L_1 of the discrete heat source, in addition to its dependence on various other parameters as well. It is therefore imperative to discretize the computational domain such that it mirrors the physics of the problem accurately. There should always be a certain minimum number of closely packed grids near the leading edge of the board from where the flow begins. A certain minimum number of finer grids is needed along the discrete heat source as well, owing to the fact that the temperature gradients will be larger there. The grid pattern along the board, beyond the heat source, depends on the location of the heat source itself. In the extended region, beyond the board, it suffices to have grids, which become gradually coarse. Perpendicular to the board, it is adequate to have grids that are closely spaced near the board and become gradually coarse away from the board. In view of the above prerequisites the grid pattern has to satisfy, a hybrid grid system has been evolved. Based on the results of a grid sensitivity test to be presented later, a grid size of 121×121 has been used. A semicosine function is chosen for generating the grids perpendicular to the board (in the Y direction). Along the board, cosine grids are used from the leading edge up to the discrete heat source, while semicosine grids are used along the discrete heat source. Beyond the heat source, up to the trailing edge of the board, the grids are generated using geometric progression. In the extended domain, in the X direction, always a fixed number of 21 grids, generated using geometric progression, are used, while there is no change in the grid pattern in the Y direction.

METHOD OF SOLUTION

The normalized governing equations [Eqs. (7)–(9)] are nonlinear partial differential equations, the solution for which is evolved in two stages. The first stage involves transforming the governing equations into finite-difference equations using a finite-volume-based finite-difference method of Gosman et al. [14]. The advection terms in Eqs. (7) and (9) are tackled using second upwinding. The resulting algebraic equations, together with the boundary conditions, are solved in the subsequent stage using the Gauss-Seidel iterative procedure. Underrelaxation (relaxation parameter = 0.5) is used on stream function (ψ) and vorticity (ω), while full relaxation (relaxation parameter = 1) is used on temperature (θ). Very stringent convergence criteria (δ_c) of 5×10^{-6}, 1×10^{-6}, and 1×10^{-6} have been imposed on vorticity (ω),

stream function (ψ), and temperature (θ), respectively. Three-point formulas, using a second-degree Lagrangian polynomial, are used for evaluating all the derivatives present in all the boundary conditions, and also those derivatives that are needed in the rest of the calculations. The integrations required in all the calculations are performed using the extended Simpson's 1/3 rule for nonuniform step sizes. The velocities and temperatures in the entire computational domain [including nondimensional local board temperatures, $\theta_p(X)$] are obtained as part of the solution. The nondimensional maximum board temperature ($\theta_{\max}$) is determined from the local values of nondimensional temperature along the board. The nondimensional average board temperature is evaluated as $\theta_{\text{av}} = \int_0^1 \theta_P \, dX$. The net convection heat transfer rate from the board is calculated as $Q_C = -k_f \Delta T_{\text{ref}} \int_0^1 (\partial\theta/\partial Y)_{Y=0} \, dX$. The net radiation heat transfer rate from the board is obtained as $Q_R = \varepsilon N_{RF} k_f \Delta T_{\text{ref}} \int_0^1 \left\{ [1 + \theta_P(\Delta T_{\text{ref}}/T_\infty)]^4 - 1 \right\} dX$. The mean friction coefficient is determined as $\overline{C}_f = (2/\text{Re}_L) \int_0^1 \left(\frac{\partial U}{\partial Y}\right)_{Y=0} dX$.

All the calculations are performed using air ($\text{Pr} = 0.71$) as the cooling agent. The height of the electronic board (L) is taken to be 233.4 mm, which is typical of a printed circuit board in practice. The thickness of the board (t) is taken equal to 1.5 mm while the height of the discrete heat source (L_h) is taken equal to 1/8th the board height (i.e., 29.2 mm). The heat source position is varied from the leading edge ($A_1 = 0$) to the trailing edge ($A_1 = 0.875$) of the board, where A_1 is the nondimensional position of the heat source given as (L_1/L). The thermal conductivity of the board material is varied between 0.25 and 1 W/m K, keeping in mind that the thermal conductivity of electronic boards is typically of the order of unity (e.g., epoxy glass, with $k_s \approx 0.26$ W/m K). The board surface emissivity is varied between 0.05 (a good reflector, e.g., polished aluminum foil) and 0.85 (a good emitter, e.g., black paint). Before deciding on the appropriate range for Ri_L^*, the problem has been solved for different values of $\text{Ri}_L^* = 2, 500, 250, 25, 1, 0.25$, and 0.1, for a typical case with $q_v = 10^6$ W/m^3, $k_s = 0.25$ W/m K, and $\varepsilon = 0.85$. The nature of variation of the maximum board temperature ($\theta_{\max}$) with the position of the heat source (A_1) has been studied for all the above values of Ri_L^*. No significant change has been observed in $\theta_{\max}$ between $\text{Ri}_L^* = 2{,}500$ and 25. For example, for $A_1 = 0$, $\theta_{\max}$ decreases by only 3.3% as Ri_L^* decreases from 2,500 to 25. However, the decrease in $\theta_{\max}$ has been found to be fairly large toward lower values of Ri_L^*. For example, for $A_1 = 0$, $\theta_{\max}$ decreases by as much as 14.5% as Ri_L^* decreases from 0.25 to 0.1. The trends have been observed to be similar for other positions of the heat source and for other surface emissivities as well. Therefore, from the point of view of $\theta_{\max}$, which is of prime interest in applications such as cooling of electronic equipment, $0.1 \le \text{Ri}_L^* \le 25$ has been considered the most appropriate range for Ri_L^* in all calculations.

RESULTS AND DISCUSSION

Grid-Independence Test

To study the effect of grid size ($M \times N$) on the solution, a typical case with $q_v = 5 \times 10^5$ W/m^3, $A_1 = 0.4375$ (heat source located at the center of the board),

$k_s = 0.25$ W/m K, $\epsilon = 0.45$, $\mathrm{Re}_L = 1{,}275$, and $\mathrm{Ri}_L^* = 1$ has been considered. The grid independence has been tested in two stages—first with M fixed (to decide on the value of N) and later with N fixed (to decide on the value of M). The results of the above test are summarized in Table 1. The first stage of the study shows that the difference in $\theta_{\max}$ between grid sizes 121×121 and 121×141 is only 0.06%, while the difference in $\overline{C}_f$ between the same grid sizes is 0.62%. The results of the second stage of the grid-independence test performed keeping N fixed reveal that the differences in the values of $\theta_{\max}$ and $\overline{C}_f$ between grid sizes 121×121 and 141×121 are 0.07% and 0.54%, respectively. In view of the above, M and N have both been fixed as 121 for all the subsequent calculations pertaining to the present study.

Effect of Height and Width of the Computational Domain

To analyze the role the height (H) of the computational domain plays in the present problem, results have been obtained for the same typical case as considered in the foregoing grid-independence test, by solving the problem with computational domains of different heights. It has been noticed that the difference in $\theta_{\max}$ between $H/L = 2$ and $= 2.5$ is 0.71%, while the difference in $\overline{C}_f$ between the same two values of H/L is only 0.04%. Because of these results, a computational domain of height $H = 2L$ has been used for all the subsequent computations for this problem. With regard to width (W) of the computational domain, similar studies have been made and a value of $W = L$ has been found to be adequate for making calculations.

Testing the Results for Mass and Energy Balance

The results of the present problem have been tested for mass and energy balance. This is done by comparing the mass inflow with the mass outflow and the total rate of heat transfer by mixed convection and surface radiation with the total rate at which heat is generated in the heat source, respectively. A typical case with $q_v = 5 \times 10^5$ W/m^3, $k_s = 0.5$ W/m K, $\epsilon = 0.45$, $\mathrm{Re}_L = 2{,}250$, and $\mathrm{Ri}_L^* = 1$ has been considered. As many as 13 different locations for the heat source ($0 \le A_1 \le 0.875$) are chosen, starting from the leading edge to the trailing edge of the electronic board. The mass balance and the energy balance are found to be satisfactory, with the

Table 1. Grid-independence test to decide the values of M and N[a]

Stage	Grid size, $M \times N$	$\theta_{\max}$	Percentage change (abs.)	$\overline{C}_f$	Percentage change (abs.)
(1) M fixed at 121,	121×101	1.0429	—	0.0642	—
N varied	121×121	1.0348	0.78	0.0648	0.86
	121×141	1.0355	0.06	0.0644	0.62
(2) N fixed at 121,	101×121	1.0357	—	0.0652	—
M varied	121×121	1.0348	0.09	0.0648	0.57
	141×121	1.0341	0.07	0.0644	0.54

[a] $L = 233.4$ mm, $t = 1.5$ mm, $L_h = 29.2$ mm, $A_1 = 0.4375$, $q_v = 5 \times 10^5$ W/m^3, $k_s = 0.25$ W/m K, $\varepsilon = 0.45$, $k_f = 0.03$ W/m K, $\mathrm{Re}_L = 1{,}275$, and $\mathrm{Ri}_L^* = 1$.

maximum deviations limited to $\pm 0.008\%$ and $\pm 3.92\%$, respectively. Similar observations hold with regard to other cases considered in the present study.

Validation

The fluid flow and heat transfer results of the present problem are validated with available analytical results in the asymptotic limits. In order to be able to do this, the present complex problem of an electronic board with longitudinally varying surface temperature (owing to discrete internal heat generation followed by conduction with subsequent convection and surface radiation) is degenerated to the limiting case of an isothermal electronic board. Later, the results for the asymptotic forced-convection limit are verified against the well-known exact solutions of Blasius [15] and Pohlhausen [16]. The calculations in the asymptotic free-convection limit are validated with the exact solution of Ostrach [17]. The mean friction coefficient calculation is validated with that of Blasius [15] in the asymptotic forced-convection limit.

Validation for velocity and temperature. The nondimensional vertical velocity (U) and temperature (θ) profiles at the trailing edge of the electronic board are compared with those of Blasius [15] and Pohlhausen [16] in the asymptotic forced-convection limit ($\mathrm{Ri}_L = 10^{-5}$), as shown in Figure 3*a*. In the asymptotic free-convection limit ($\mathrm{Ri}_L = 10^5$), on the other hand, the comparison is made with reference to Ostrach [17], as shown in Figure 3*b*. The above two plots [Figure 3*a* and 3*b*] are drawn for $\mathrm{Pr} = 1$. The figures reveal that the present results, though obtained for the asymptotic limiting cases, are in fairly good agreement with the forced-convection and free-convection results of Blasius-Pohlhausen and Ostrach, respectively.

Validation for mean friction coefficient. The validation for $\overline{C}_f$ has been done for the asymptotic forced-convection limit ($\mathrm{Ri}_L = 10^{-5}$) with the exact solution of Blasius [15]. Excellent agreement between the two has been found. Also, based on a set of 21 data, obtained from the present study, encompassing a wide range of Reynolds numbers ($0.016 \times 10^5 \leq \mathrm{Re}_L \leq 1.6 \times 10^5$), a single-variable correlation for $\overline{C}_f$ has been developed as $\overline{C}_f = 1.276\,\mathrm{Re}_L^{-0.5}$. The $\overline{C}_f$ determined from this correlation differs from that obtained using the Blasius solution [$\overline{C}_f = 1.328\,\mathrm{Re}_L^{-0.5}$] by only 3.9% for all Reynolds numbers.

Validation for local Nusselt number. In order to further validate the heat transfer results of the present problem for the limiting case of an isothermal electronic board, a local Nusselt number Nu_x has been defined as $\mathrm{Nu}_x = (h_x x/k)$. Figure 4 shows the variation of local Nusselt number (Nu_x) along the electronic board for the case with $\mathrm{Pr} = 1$ and $\mathrm{Gr}_L = 10^6$ in the asymptotic forced- and free-convection limits, with $\mathrm{Ri}_L = 10^{-5}$ and 10^5, respectively. The figure shows absolute agreement between the present results and the exact analytical solution of Pohlhausen [16] and Ostrach [17], respectively. It can also be observed that the local Nusselt number (Nu_x) decreases monotonically along the board from the leading edge to the trailing edge

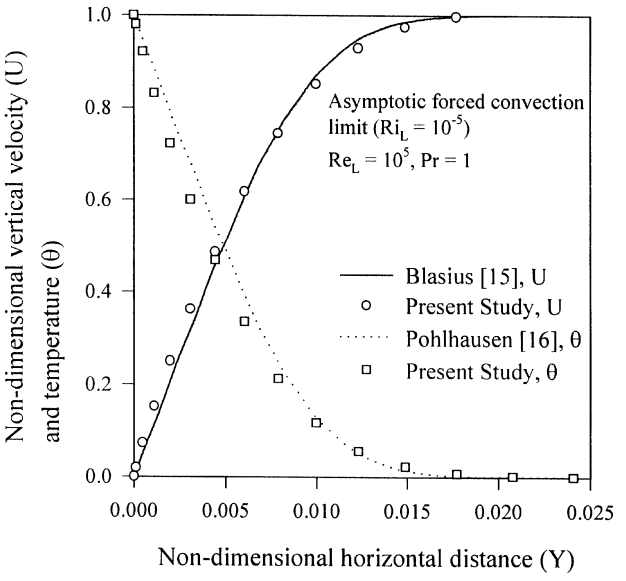

(a)

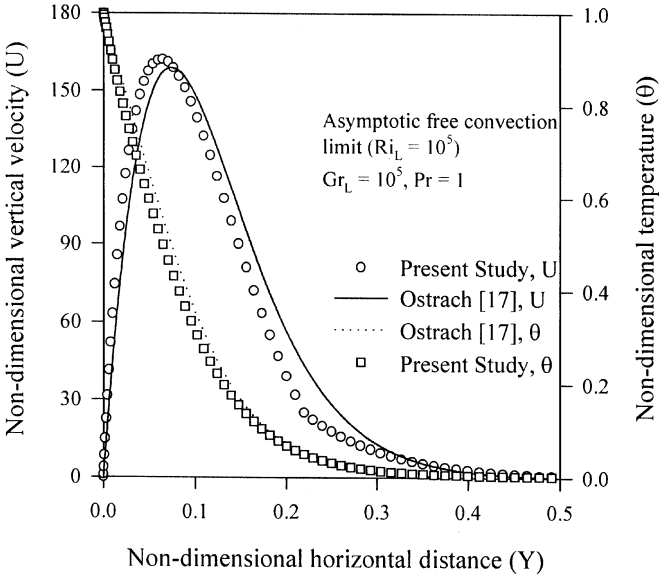

(b)

Figure 3. Comparison of nondimensional vertical velocity and temperature profiles from the present study with available analytical results in the asymptotic (*a*) forced and (*b*) free-convection limits.

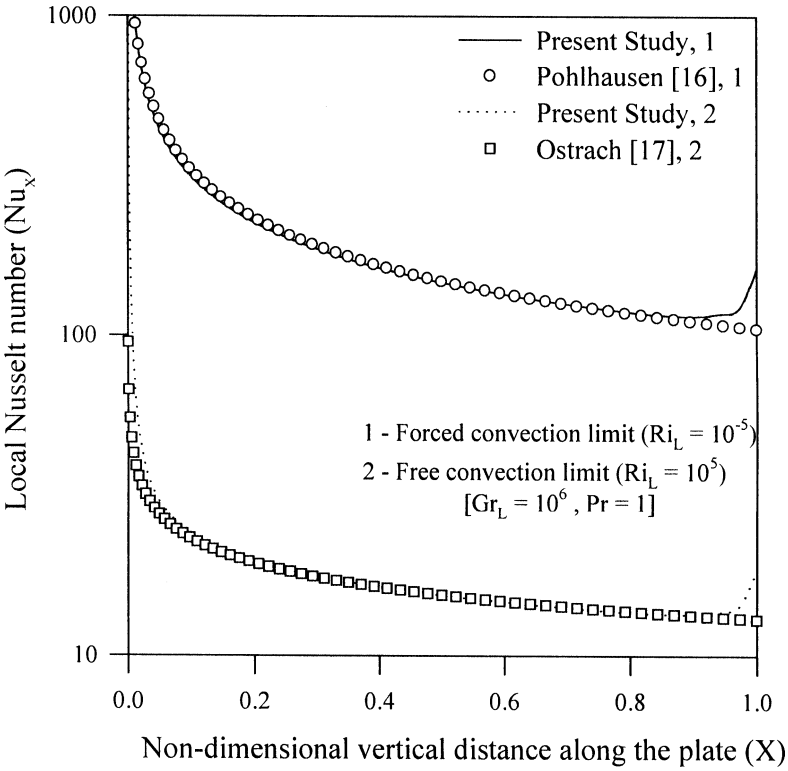

Figure 4. Comparison of local Nusselt number along the board in the asymptotic forced- and free-convection limits with the available analytical results.

in both cases. A small increase in Nusselt number near the trailing edge can be seen in the results of the present study, which could be attributed to the sudden change in the temperature boundary condition along the left free (or open) extended boundary, beyond the trailing edge of the board.

Variation of Local Board Temperature with Other Parameters

Temperature distribution along the board is of prime interest in the present problem. This depends on the rate of volumetric heat generation in the discrete heat source (q_v), the location of the heat source (L_1), the thermal conductivity (k_s), the surface emissivity (ϵ), and the free-stream velocity (u_∞) (or, in other words, Ri_L^*).

Figure 5 shows the local board temperature [$\theta_P(X)$] profiles for the case where the heat source is positioned at the center of the board (i.e., $A_1 = 0.4375$), with $q_v = 5 \times 10^5$ W/m^3, $k_s = 0.5$ W/m K and $\epsilon = 0.85$. The free-stream velocity is varied to cover four values of Ri_L^* (viz., 25, 1, 0.25, and 0.1). From the figure, it can be seen that the board temperature increases gently near the leading edge and then rises sharply to a maximum at a location near the center of the board. Again, the temperature drops sharply to some lower value, and from there on, it undergoes an asymptotic decrease toward the trailing edge of the board. The temperature will be

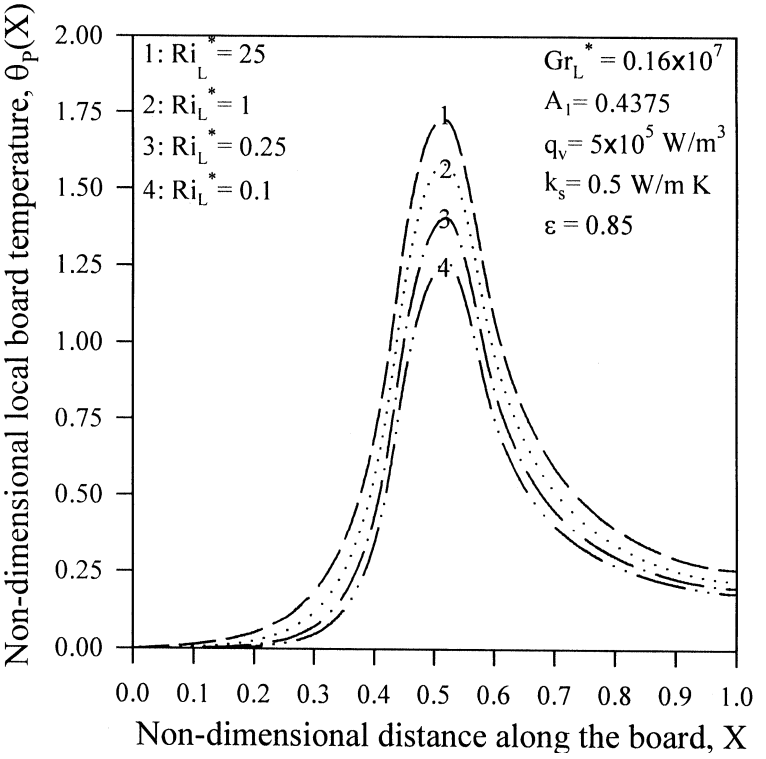

Figure 5. Nondimensional local board temperature profiles for a given heat source position and for different Richardson numbers.

reasonably large even at the trailing edge of the board. Further, excluding some initial distance from the leading edge, where the temperatures are very close to the ambient, temperature at any location along the board decreases with increasing Re_L or (decreasing Ri_L^*). This is because of the increase in the rate of convection heat transfer as one moves from the free-convection-dominant regime ($\mathrm{Ri}_L^* = 25$) to the forced-convection-dominant regime ($\mathrm{Ri}_L^* = 0.1$). For example, the peak board temperature comes down by about 29% as Ri_L^* decreases from 25 to 0.1, with all other parameters held fixed, in the specific example considered in Figure 5.

Figure 6 shows a family of local board temperature profiles for the case with the same values of A_1, q_v, and k_s as in Figure 5, but with u_∞ chosen such that, for all the curves, $\mathrm{Re}_L = 250$ and $\mathrm{Ri}_L^* = 25$. The plots are drawn for three different values of surface emissivity (viz., $\epsilon = 0.05$, 0.45, and 0.85). The figure shows that at any given location along the board, the temperature decreases with ϵ. This is because the rate of heat transfer by radiation increases with ϵ, thus bringing down the board temperature. For example, the peak temperature in the board decreases by about 28% as its surface emissivity (ϵ) increases from 0.05 to 0.85.

It is to be noted that all the curves in Figures 5 and 6 correspond to a single position of the discrete heat source, wherein the heat source is located at the board centre (i.e., $A_1 = 0.4375$). In view of this, a family of curves has been drawn, as shown

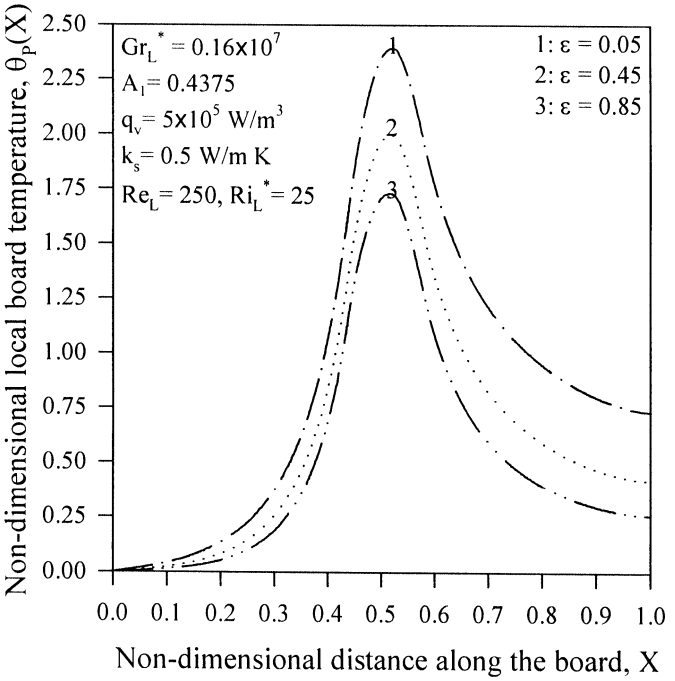

Figure 6. Nondimensional local board temperature profiles for a given Richardson number and for different surface emissivities.

in Figure 7, depicting the nature of variation of local temperature $[\theta_P(X)]$ along the board, for five different positions of the discrete heat source, viz., A_1 [or (L_1/L)] = 0, 0.05, 0.4375, 0.825, and 0.875. The curves pertaining to Figure 7 are plotted for the case with $q_v = 10^5$ W/m^3, $k_s = 0.5$ W/m K, $\epsilon = 0.45$, $Re_L = 1{,}800$, and $Ri_L^* = 0.1$. It can be seen from the figure that the value of the maximum board temperature, as well as the location at which the maximum occurs, will vary with the position (A_1) of the heat source. Further, the peak temperature increases as the heat source is traversed from the leading edge to the trailing edge of the board.

Variation of Maximum Board Temperature with Other Parameters

A study of the variation of maximum board temperature (θ_{max}) with the position of the discrete heat source along the board indicates the best possible location for the heat source from the viewpoint of minimizing the maximum temperature attained by the board under a given set of operating conditions.

In this context, Figure 8 shows a family of curves giving the variation of θ_{max} with A_1 for four values of free-stream velocity (and hence four values of Ri_L^*, viz., 25, 1, 0.25, and 0.1). It may be noted that A_1 represents the position of the beginning of the discrete heat source, and the maximum possible value for A_1 is 0.875. It may also be noted that the plot does not indicate the location along the board at which θ_{max}

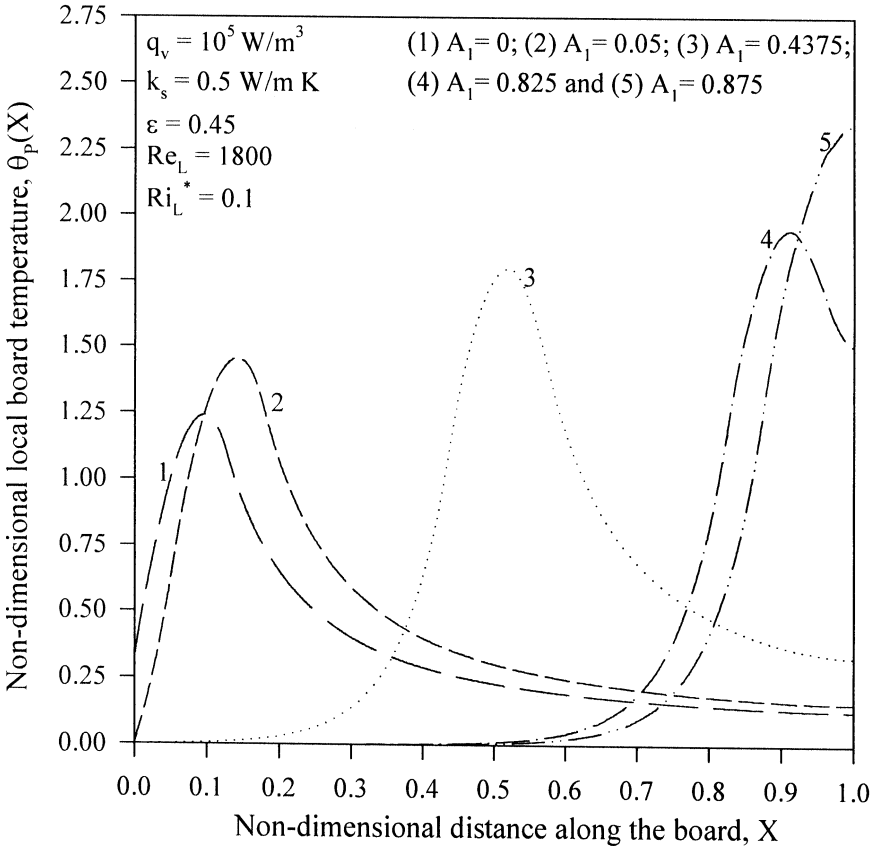

Figure 7. Nondimensional local board temperature profiles for a given Richardson number and for different positions of the heat source along the board.

occurs. Instead, it gives the values of θ_{max} the board assumes for different positions of the heat source. These curves correspond to $q_v = 10^6$ W/m^3, $k_s = 0.25$ W/m K, and $\epsilon = 0.85$. From the figure, it is clear that there is a sharp increase in θ_{max} from $A_1 = 0$ to $A_1 = 0.05$ and again from $A_1 = 0.825$ to $A_1 = 0.875$. There is a considerably slower rate of increase in θ_{max} for A_1 between 0.05 and 0.825. As Ri_L^* decreases from 25 to 0.1, the amount by which θ_{max} increases between the positions $A_1 = 0.05$ and $A_1 = 0.825$ also increases. In the case considered here, the increase in θ_{max}, between $A_1 = 0.05$ and $A_1 = 0.825$, for $Ri_L^* = 25$, is only 6.5%, while that for $Ri_L^* = 0.1$ is about 24%. The figure also shows that θ_{max} decreases with increasing u_∞ (and hence increasing Re_L) or decreasing Ri_L^*, for any given position A_1, for reasons already given. The figure clearly indicates that the best possible position for the heat source is $A_1 = 0$ (the leading edge of the board), as would be expected. The least preferred position is $A_1 = 0.875$ (the heat source ending on the trailing edge of the board) for all values of Ri_L^*. In the present example, for $Ri_L^* = 0.1$ (asymptotic forced convection limit for this problem), θ_{max} increases by as much as 51% as the heat source moves from $A_1 = 0$ to $A_1 = 0.875$. Similar trends are observed for other values of Ri_L^* as well.

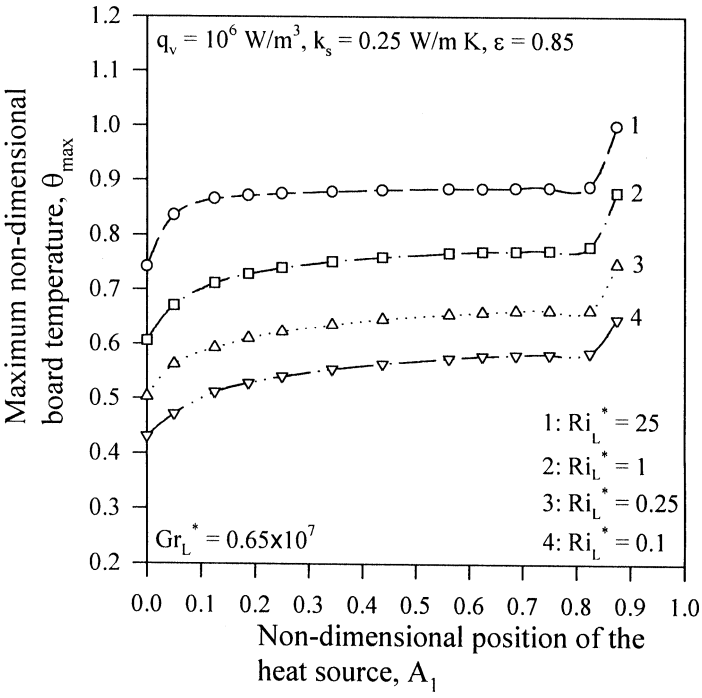

Figure 8. Variation of maximum nondimensional board temperature with Richardson number for various positions of the heat source along the board.

To study the effect of surface emissivity (ϵ) of the electronic board on θ_{max} in the range of Richardson numbers ($0.1 \leq Ri_L^* \leq 25$) considered in the present study, a set of curves has been drawn as shown in Figure 9. These curves pertain to the case with $q_v = 10^6$ W/m^3, $k_s = 0.25$ W/m K, and are plotted for three values of Ri_L^* (viz., 25, 1, and 0.1) and two values of ϵ (viz., 0.05 and 0.85). It can be seen from the figure that θ_{max} decreases as ϵ increases for a given Ri_L^* (or u_∞). In the example taken here, for $Ri_L^* = 1$, θ_{max} for $A_1 = 0$ decreases by 17%, while that for $A_1 = 0.875$ decreases by 25%, as ϵ increases from 0.05 to 0.85. Another important feature is that the effect of ϵ on θ_{max} is more pronounced in the free-convection-dominant regime ($1 < Ri_L^* \leq 25$) than in the forced-convection-dominant regime ($0.1 \leq Ri_L^* \leq 1$). In the present example, for $Ri_L^* = 25$ (asymptotic free convection limit), θ_{max} for $A_1 = 0.875$ decreases by as much as 27.9% as ϵ increases from 0.05 to 0.85. While for $Ri_L^* = 0.1$ (asymptotic forced-convection limit), θ_{max} for the same heat source position (viz., $A_1 = 0.875$) decreases by a smaller percentage of 17.8% as ϵ increases between the same limits (i.e., from 0.05 to 0.85).

Relative Contributions of Convection (Free and Forced) and Surface Radiation to Heat Dissipation from the Electronic Board

The heat generated in the discrete heat source is dissipated from the right surface of the board by convection (which includes free and forced convection) and

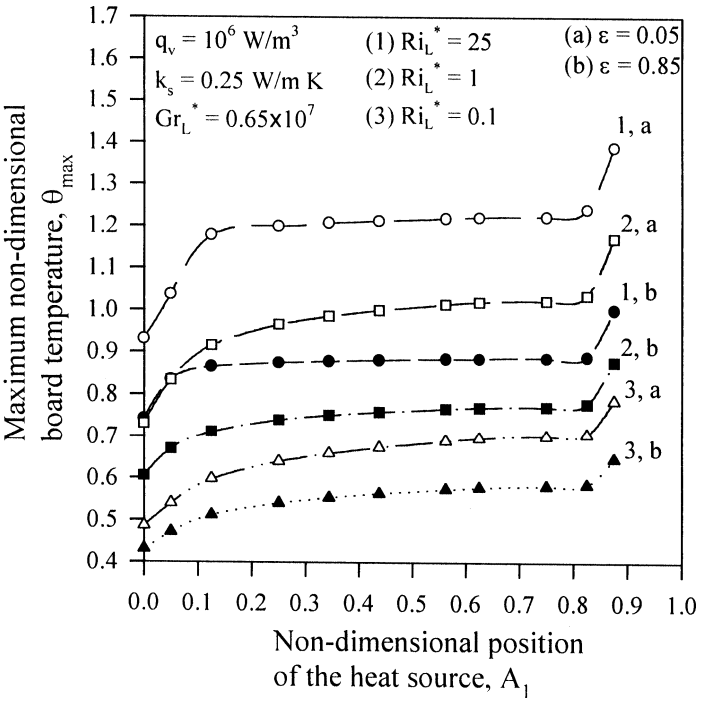

Figure 9. Variation of maximum nondimensional board temperature with surface emissivity for various positions of the heat source along the board.

surface radiation. It is interesting to study the role that radiation plays in comparison to convection in the present problem.

Figure 10 shows the relative contributions of convection and radiation, drawn against A_1, for $Ri_L^* = 25$, 1, and 0.1, for the case $q_v = 10^6$ W/m^3, $k_s = 0.25$ W/m K, and $\epsilon = 0.85$. The most striking feature that is noticeable from Figure 10 is the behavior of the two curves pertaining to $Ri_L^* = 25$ (asymptotic free-convection limit). It is seen that convection heat transfer decreases from 45% for $A_1 = 0$ to about 41.5% for $A_1 = 0.05$, but from then increases monotonically to a maximum of 65% for $A_1 = 0.875$. An exact mirror-image variation is noticed for radiation, which increases from 55% for $A_1 = 0$ to about 58.5% for $A_1 = 0.05$, and then decreases monotonically to a minimum of 35% for $A_1 = 0.875$. These two curves cross each other at $A_1 = 0.625$, which denotes equal contributions to heat transfer by convection and radiation. Similar trends are observed for $Ri_L^* = 1$ and 0.1. Figure 10 also clearly shows the role that surface radiation plays in all three (free-convection-dominant, mixed-convection-dominant, and forced-convection dominant) regimes. As expected, there is a continuous decrease in the contribution from radiation as one moves from the asymptotic free-convection limit to the asymptotic forced-convection limit. In the present example, in the asymptotic free-convection limit ($Ri_L^* = 25$), radiation is significant, with maximum and minimum contributions of 58.5% and 35%, respectively, depending on the position (A_1) of the heat source. Even in the asymptotic forced-convection

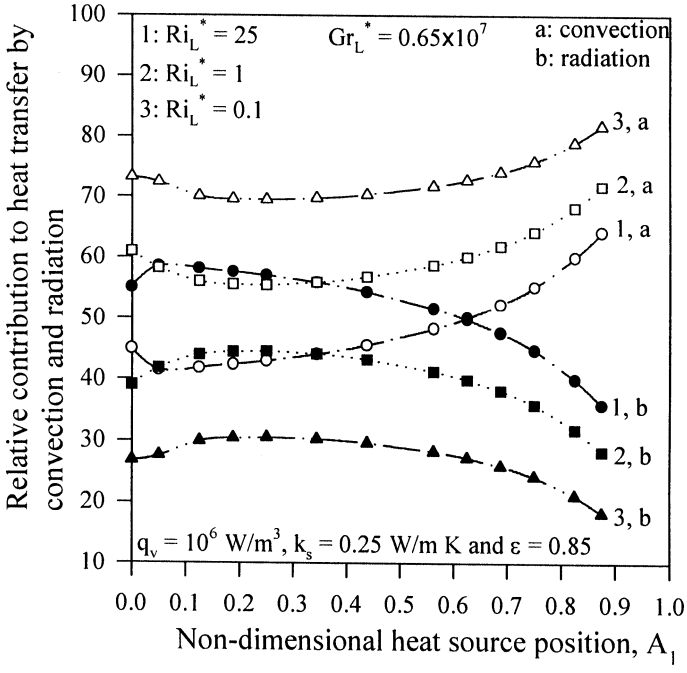

Figure 10. Variation of relative contributions of convection and surface radiation to heat dissipation from the board with heat source position in different regimes of mixed convection.

limit ($\mathrm{Ri}_L^* = 0.1$), where convection is expected to override radiation, the latter plays a fairly important role, with maximum and minimum contributions of 30.5% and 18.5%, respectively. In the mixed-convection regime (i.e., $\mathrm{Ri}_L^* = 1$), the maximum and minimum contributions of radiation fall in between those for the above two extremes. They have been found to vary between 44.5% and 28.3%, respectively, in the present example, depending the position of the heat source along the board.

To isolate the role of radiation further, the present problem has been solved for three typical surface emissivities ($\epsilon = 0.05$, 0.45, and 0.85) for the case $q_v = 10^6$ W/m^3, $k_s = 0.25$ W/m K, $\mathrm{Re}_L =$ 2,500, and $\mathrm{Ri}_L^* = 1$. The results are shown in Figure 11. It can be seen that the dominant mode of heat transfer for $\epsilon = 0.05$ (a good reflecting surface, such as polished aluminum) is convection, with very little contribution from radiation. In the present example, for the case where the heat source is located at the center of the board ($A_1 = 0.4375$), for $\epsilon = 0.05$, convection takes away as much as 96% of the heat generated, while radiation contributes to a mere 4%. The contribution by radiation increases with emissivity, with a proportionate decrease in that by convection. In the present example, for the case where the heat source is positioned at $A_1 = 0.25$, the radiation heat transfer is 4.5% only for $\epsilon = 0.05$. It increases to 30% for $\epsilon = 0.45$, while, for $\epsilon = 0.85$, the radiation contribution is as much as 45%, implying a 10-fold increase compared to the case of $\epsilon = 0.05$.

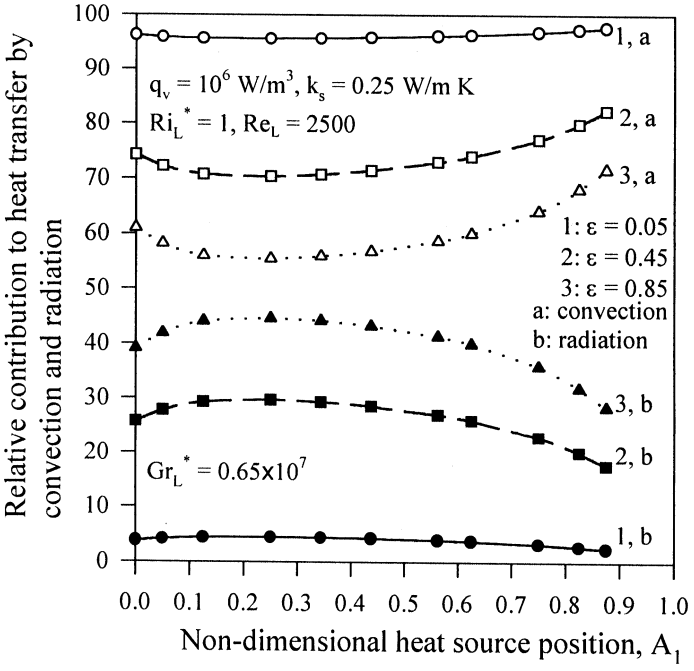

Figure 11. Variation of relative contributions of convection and surface radiation to heat dissipation from the board with heat source position for different surface emissivities.

CONCLUSIONS

An exhaustive numerical study of the problem of buoyancy-aided mixed convection, with conduction and surface radiation, from a vertical electronic board, possessing a flush-mounted, traversable discrete heat source, has been made. From the viewpoint of minimizing the maximum board temperature, the best position for the heat source is the leading edge of the board, and the maximum board temperature increases as the heat source moves away from the leading edge. The least advisable position for the heat source is the trailing edge of the board, as it is found to increase θ_{max} by 35–50%, when compared to that for the case where the heat source starts from the leading edge of the board. The peak temperature, for any Ri_L^* and for given values of q_v and k_s, decreases with increasing ϵ. However, the degree of decrease of θ_{max} with ϵ decreases as one moves from the free-convection limit ($Ri_L^* = 25$) to the forced-convection limit ($Ri_L^* = 0.1$). Radiation is found to assume a significant role in all regimes of mixed convection. For example, for $\epsilon = 0.85$, for $Ri_L^* = 25$, radiation contributes 35–60% to heat transfer, depending on heat source position. For the same $\epsilon = 0.85$, for $Ri_L^* = 1$ and 0.1, the radiation contributions have been found to be 28–45% and 18–30%, respectively. For a given Ri_L^*, convection is found to play a dominant role, taking away as much as 90–95% of the heat in the case of a good reflecting surface ($\epsilon = 0.05$), with radiation having an insignificant role. However, the radiation contribution increases with ϵ for the same Ri_L^*. It may be as much as 45–50%, depending on the heat source position, for a good emitting surface ($\epsilon = 0.85$).

REFERENCES

1. A. E. Zinnes, The Coupling of Conduction with Laminar Natural Convection from a Vertical Flat Plate with Arbitrary Surface Heating, *ASME J. Heat Transfer*, vol. 92, pp. 528–534, 1970.
2. S. S. Tewari and Y. Jaluria, Mixed Convection Heat Transfer from Thermal Sources Mounted on Horizontal and Vertical Surfaces, *ASME J. Heat Tansfer*, vol. 112, pp. 975–987, 1990.
3. M. A. Gorski and O. A. Plumb, Conjugate Heat Transfer from an Isolated Heat Source in a Plane Wall, *Proc. Winter Annual Meeting of the American Society of Mechanical Engineers*, ASME HTD–210, pp. 99–105, 1992.
4. K. Kishinami, H. Saito, and J. Suzuki, Combined Forced and Free Laminar Convective Heat Transfer from a Vertical Plate with Coupling of Discontinuous Surface Heating, *Int. J. Numer. Meth. Heat Fluid Flow*, vol. 5, pp. 839–851, 1995.
5. K. Kishinami, H. Saito, J. Sujuki, A. H. H. Ali, H. Umeki, and N. Kitano, Fundamental Study of Combined Free and Forced Convective Heat Transfer from a Vertical Plate Followed by a Backward Step, *Int. J. Numer. Meth. Heat Fluid Flow*, vol. 8, pp. 717–736, 1998.
6. M. A. Hossain and H. S. Takhar, Radiation Effect on Mixed Convection along a Vertical Plate with Uniform Surface Temperature, *Heat Mass Transfer/Waerme- und Stoffuebertr.*, vol. 31, pp. 243–248, 1996.
7. M. Vynnycky, and S. Kimura, Conjugate Free Convection due to a Heated Vertical Plate, *Int. J. Heat Mass Transfer*, vol. 39, pp. 1067–1080, 1996.
8. J. H. Merkin and I. Pop, Conjugate Free Convection on a Vertical Surface, *Int. J. Heat Mass Transfer*, vol. 39, pp. 1527–1534, 1996.
9. K. D. Cole, Conjugate Heat Transfer from a Small Heated Strip, *Int. J. Heat Mass Transfer*, vol. 40, pp. 2709–2719, 1997.
10. H. Y. Wang, F. Penot, and J. B. Sauliner, Numerical Study of a Buoyancy-Induced Flow along a Vertical Plate with Discretely Heated Integrated Circuit Packages, *Int. J. Heat Mass Transfer*, vol. 40, pp. 1509–1520, 1997.
11. S. Kimura, A. Okajima, and T. Kiwata, Conjugate Natural Convection from a Vertical Heated Slab, *Int. J. Heat Mass Transfer*, vol. 41, pp. 3203–3211, 1998.
12. F. Mendez and C. Trevino, The Conjugate Conduction-Natural Convection Heat Transfer along a Thin Vertical Plate with Non-uniform Internal Heat Generation, *Int. J. Heat Mass Transfer*, vol. 43, pp. 2739–2748, 2000.
13. C. Gururaja Rao, C. Balaji, and S. P. Venkateshan, Numerical Study of Laminar Mixed Convection from a Vertical Plate, *Int. J. Transport Phenomena*, vol. 2, pp. 143–157, 2000.
14. A. D. Gosman, W. M. Pun, A. K. Runchal, D. B. Spalding, and M. Wolfshtein, *Heat and Mass Transfer in Recirculating Flows*, pp. 89–137, Academic Press, New York, 1969.
15. H. Blasius, Grenzschichten in Flussigkeiten mit kleiner Reibung, *Z. Math. Phys.*, vol. 56, p. 1, 1908.
16. E. Pohlhausen, Der Warmeaustausch Zwischen festen Korpern und Flussigkeiten mit kleiner Warmeleitung, *Z. Angew. Math. Mech.*, vol. 1, p. 115, 1921.
17. S. Ostrach, An Analysis of Laminar Free Convection Flow and Heat Transfer about a Flat Plate Parallel to the Generating Body Force, Rep. NACA-1111, 1953.